Cement and Concrete Research 79 (2016) 373–385

Contents lists available at ScienceDirect

Cement and Concrete Research

journal homepage: http://ees.elsevier.com/CEMCON/default.asp

Chloride-induced corrosion of steel in cracked concrete – Part I: Experimental studies under accelerated and natural marine environments

M. Otieno [a,*], H. Beushausen [b], M. Alexander [b]

[a] School of Civil and Environmental Engineering, University of the Witwatersrand, Johannesburg, Private Bag 3, 2050 Wits, South Africa
[b] Department of Civil Engineering, University of Cape Town, Private Bag X3, 7701 Rondebosch, South Africa

ARTICLE INFO

Article history:
Received 28 July 2014
29 June 2015
Accepted 6 August 2015
Available online 6 November 2015

Keywords:
Corrosion rate prediction
chloride-induced corrosion
accelerated corrosion
natural corrosion
cracked concrete

ABSTRACT

Parallel corrosion experiments were carried out for 2¼ years by exposing one half of 210 beam specimens (120 × 130 × 375 mm long) to accelerated laboratory corrosion (cyclic wetting and drying) while the other half underwent natural corrosion in a marine tidal zone. Experimental variables were crack width w_{cr} (0, incipient crack, 0.4, 0.7 mm), cover c (20, 40 mm), binder type (PC, PC/GGBS, PC/FA) and w/b ratio (0.40, 0.55). Results show that corrosion rate (i_{corr}) was affected by the experimental variables in the following manner: i_{corr} increased with increase in crack width, and decreased with increase in concrete quality and cover depth. The results also show that the corrosion performance of concretes in the field under natural corrosion cannot be inferred from its performance in the laboratory under accelerated corrosion. Other factors such as corrosion process should be taken into account.

1. Introduction

Corrosion of steel reinforcement is one of the main deterioration mechanisms for reinforced concrete (RC) structures in temperate, marine, and industrial environments. It has become a major durability concern for both asset owners and engineers. If left unabated, it accelerates the deterioration of RC structures and may lead to several interrelated negative consequences including, but not limited to, cracking and spalling of concrete cover, loss of steel cross-section area, degradation of steel-concrete interface bond, and ultimately reduction in service life of the RC structure. In addition, it requires high expenditures for maintenance, repair or replacement, and compromises public safety. Even though corrosion of steel in RC structures can be caused mainly by either ingress of carbon dioxide (carbonation-induced) or chlorides (chloride-induced), the latter is the chief cause of steel corrosion in RC structures. Notably, chloride-induced corrosion causes widespread damage of the RC structure and may ultimately result in failure (depending on the pre-defined limit state) within a relatively short period of time (before the structure meets its target service life).

In the presence of cracks in concrete, the aggressive nature of chloride-induced corrosion and the related rate of deterioration of the RC structure are exacerbated. Cracks impair the durability of RC structures by creating preferential paths for the penetration of corrosion-inducing species (H_2O, O_2, CO_2, Cl^-) [1,2] leading to relatively faster initiation and propagation of steel corrosion and consequently a reduction in service life . If no cracks are present, both the initiation and propagation phases are usually a function of, among other factors, the penetrability of the concrete cover, the cover thickness, resistivity of concrete, and the corrosion resistance of the steel bars [3–5]. In the presence of cracks, studies have shown that the factors affecting corrosion rate in uncracked concrete are still relevant but their effectiveness is significantly reduced [4–9]. The effects of cracks on corrosion vary not only with their width, but also with depth, frequency, orientation (relative to the steel reinforcement), self-healing potential, and activity or dormancy. The study reported in this paper focused only on crack width.

Even though the effect of cover cracking on corrosion has been investigated in the past, most studies have been carried out in the laboratory under accelerated conditions (for which there are no standard test methods) mainly due to the slow nature of natural corrosion process coupled with the urgent need to provide working solutions to the corrosion problems in RC structures. Accelerated corrosion is usually achieved using several techniques including the use of impressed current [10,11], admixed chlorides [10,12], cyclic wetting and drying [13,14], and the use of simulated concrete pore solutions [15,16]. In this study, a combination of impressed current and cyclic wetting and drying were used, as will be seen in the next section. The results presented in this paper provide useful information with respect to the use of accelerated corrosion results to predict the field corrosion performance of different concretes under similar exposure conditions.

* Corresponding author. Tel.: +27 11 717 7117.
E-mail address: Mike.Otieno@wits.ac.za (M. Otieno).

http://dx.doi.org/10.1016/j.cemconres.2015.08.009
0008-8846/

2. Experimental details

2.1. Experimental variables and mix proportions

Parallel corrosion experiments were carried out by exposing one half of 210 beam specimens (120 × 130 × 375 mm) to accelerated laboratory corrosion (cyclic 3 days wetting with 5% NaCl solution followed by 4 days air-drying) while the other half were left to undergo natural corrosion in a marine tidal zone in Cape Town (Table Bay Harbour). The beams were cast using five different concretes made using two w/b ratios (0.40 and 0.55), and three binders (100% CEM I 42.5 N plain Portland cement (PC), 50/50 PC/GGBS and 70/30 PC/FA). The 0.55 w/b ratio was not used to make PC specimens. A high yield strength 10 mm diameter steel bar was embedded in each beam. A summary of the concrete mix proportions and selected concrete properties is presented in Table 1. Other experimental variables included cover depth (20 and 40 mm) and crack width (0, incipient crack, 0.4 and 0.7 mm). An incipient crack refers to a crack just induced by 3-point loading of beam specimens and thereafter unloading. Even though previous research has shown that crack widths ≤ 0.3 mm are prone to self-healing [17–19], it was not possible to quantify crack self-healing in the incipient-cracked specimens due to lack of appropriate test equipment. Further, for deeper cover depths (say 40 mm) coupled with the susceptibility to crack healing, it can be expected that incipient cracks will have negligible effect on corrosion rate. The incipient-cracked specimens were therefore made only for the laboratory and field specimens with 20 mm cover. Both ends of the steel bars were covered with electroplating tape and epoxy-coated to provide an effective exposed surface area of approximately 86 cm^2 (approximately 27.5 cm long circumferencial steel surface). Just before casting, the bars were cleaned and degreased with acetone. A 10 mm diameter × 150 mm long stainless steel bar was placed in each beam during casting (see Fig. 1) to act as a counter electrode for corrosion rate measurements.

2.2. Induction of active corrosion state

After 28-days of water-curing (at 23 ± 2 °C) and 10 days air-drying (temperature: 25 ± 2 °C, relative humidity: 50 ± 5%) in the laboratory, and prior to cracking the beam specimens, anodic impressed current (IC) was used with the intention to initiate an active corrosion rate (i.e. eliminate the corrosion initiation phase) in all the 210 beam specimens. The set-up used to initiate active corrosion in the specimens using IC is shown in Fig. 1. The theoretical time ($t_{steel\ level}$) and amount of IC required to drive the chlorides through the cover depth to the steel level was estimated using Nernst-Planck Equation in the following form: $t_{steel\ level} = c \cdot [-D(zF/RT) \cdot (\partial E/\partial x)]^{-1}$ where D is the diffusion coefficient of the ionic species (m^2/s) in concrete, z is the valence of the ionic species (-1 for Cl^-), F is Faraday's constant (96,500 C/mol), R is the universal gas constant (8.314 J/mol.K), T is the absolute temperature (298 K), c is the cover depth (20 or 40 mm) and E is the applied electrical potential (V).

The diffusion coefficient (D) was obtained was obtained from the measured 28-day chloride conductivity index (CCI) based on empirical correlations between D and CCI which take into account the effect of marine exposure environment, concrete ageing and binder type [20–22] i.e. the correlation model can estimate the time- and exposure-dependent apparent chloride diffusion coefficient for commonly used binder types (mainly plain PC, 70/30 PC/FA and 50/50 PC/GGBS) and marine exposure environments (tidal, splash and spray) in South Africa [20–22]. Part II of this paper gives more details on the determination of diffusion coefficient from the CCI. The CCI was obtained from the rapid chloride conductivity test [21,23] for each of the concrete mixes in Table 1. The 28-day and 90-day diffusion coefficients of the concretes used are presented in Table 2.

In order to determine the anodic IC required to induce active corrosion rate in the specimens of a given cover depth for each of the five concrete mixes, and after a series of iterations (of time and IC), the time to apply the IC was fixed at 1.5 hours to limit the effective applied current to less than 2.0 Amperes. The term 'effective applied current' is used here to refer to the actual applied current taking into account the corresponding 28-day measured resistance of the (water-saturated) concrete. The IC was limited to less than 2.0 Amperes to ensure chlorides reach the steel and to minimize the steel mass loss, if any. It is important to note that the applied currents were theoretically not expected to cause any steel mass loss; even though not ascertained by actual measurement of chloride content at the steel level, the objective was to drive the chlorides to the steel level within approximately 1.5 hours (taking into account cover depth and concrete quality). Beam specimens of the same binder type, w/b ratio and cover depth were connected in series, and the appropriate anodic IC applied continuously for 1.5 hours. The applied IC currents were as follows, in each case respectively for 20 mm and 40 mm cover depths: (a) PC-40: 0.03 A and 0.13 A , (b) FA-40: 0.44 A and 1.67 A, (c) FA-55: 0.25 A and 1.01 A, (d) SL-40: 0.57 A and 1.70 A, and (e) SL-55: 0.44 A and 1.67 A. After 1.5 hours, all the 72 beams were connected in series and an effective current of 8.6 μA applied for a further 2 hours – this was expected to result in a corrosion rate of approximately 0.1 $\mu A/cm^2$ in all the specimens, the assumption being that the whole exposed steel surface area of 86 cm^2 was polarized. A corrosion rate of 0.1 $\mu A/cm^2$ is conventionally taken to denote the transition from passive (initiation) to active (propagation) corrosion [24,25].

Table 1
Summary of concrete mix proportions and selected properties.

Material (kg/m^3)	Binder composition	100 % PC	50/50 PC/GGBS		70/30 PC/FA	
	w/b ratio	0.40	0.40	0.55	0.40	0.55
	Mix label	PC-40	SL-40	SL-55	FA-40	FA-55
Portland cement, PC (CEM I 42.5 N)		500	231	168	324	236
Ground granulated blastfurnace slag (GGBS)		-	231	168	-	-
Fly ash (FA)		-	-	-	139	101
Fine aggregate: Klipheuwel sand (2 mm max.)		529	749	855	749	855
Coarse aggregate: Granite (13 mm max.)		960	1040	1040	1040	1040
Water		200	185	185	185	185
Superplasticizer[a] (SP)		2.1[b] (0.4)[c]	1.8 (0.4)	0.3 (0.1)	0.4 (0.1)	-
Slump (mm)		120	105	150	85	200
28-day compressive strength (MPa)		58.2 (3.0)[d]	48.1 (2.0)	35.3 (0.9)	50.7 (0.9)	28.6 (1.9)

[a] Chemical base: Naphthalene Formaldehyde Sulphonate.
[b] Percentage of SP by mass of total binder.
[c] Amount of SP in litres/m^3.
[d] Standard deviation.

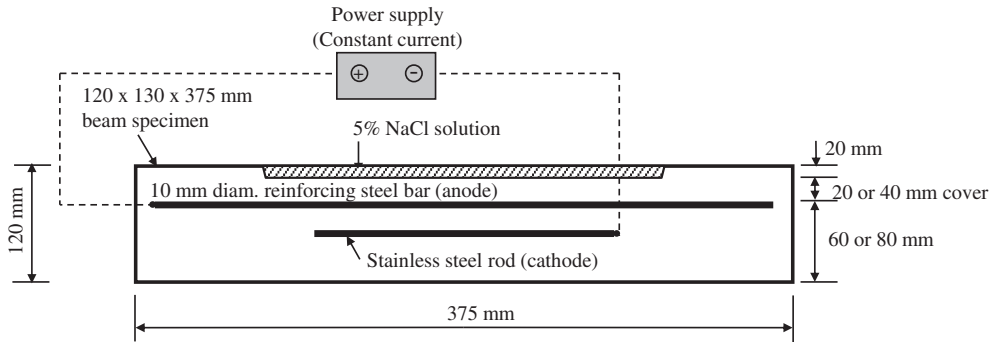

Fig. 1. Schematic of set-up to induce active corrosion in the specimens.

2.3. Crack inducing and monitoring

To facilitate the formation of a pre-corrosion transverse (flexural) crack at approximately the longitudinal centre of the beam specimens during machine loading, a 1.0 mm thick × 4 mm deep PVC sheet was placed at the centre of each beam (transversely) during casting; the PVC sheet was embedded in the beam mould, and did not remain in the beam after de-moulding at 24 hours. After induction of active corrosion, the beams (except the uncracked ones) were pre-cracked under 3-point flexural machine loading. The 0.4 and 0.7 mm cracked specimens were then placed in individual loading rigs where they remained for the entire duration of the experiments (Fig. 2). To ensure that the 0.4 and 0.7 mm crack widths remained more or less constant, demountable mechanical (demec) studs were placed on the concrete surface across the crack and the distance between the studs monitored bi-weekly using a 100 mm demec gauge. The loading rig shown in Fig. 2 was then used to adjust the crack widths as required (via the bolts and nuts).

2.4. Exposure environments

After inducing active corrosion, one half of the specimens were exposed to accelerated laboratory corrosion while the other half were left to undergo natural corrosion in a marine tidal zone.

(a) *Laboratory exposure - accelerated corrosion*
The laboratory specimens (see Fig. 3) were subjected to cycles of 3-day wetting with 5% NaCl solution followed by 4-day drying (temperature: 25 ± 2 °C and relative humidity: 50 ± 5%) throughout the experimental period.

(b) *Field exposure - natural corrosion*
The field specimens were exposed to a tidal marine zone in Cape Town (Table Bay Harbour) and left to undergo natural corrosion - see Fig. 4. The measured salinity (chloride content) of the seawater at the exposure site was approximately 2% (average of 10 samples taken at random time intervals during the experimental period, standard deviation = 0.02%). The atmospheric temperature and relative humidity around the exposure site ranged between 1 and 37 °C, and 65 and 83% respectively. The field specimens were arranged between the high and low water tide-marks in 7 rows with a total length of approximately 5 m between the seaward row (in close proximity to sea water) and inland row (in close proximity to land) (see Fig. 4). They were therefore assumed to be exposed to similar marine tidal conditions. Prior to field exposure, all the faces of the field specimens, except that with the specified cover depth, were epoxy-coated to prevent ingress of corrosion agents (Cl^-, O_2 and H_2O), and drying from those surfaces. This ensured that chlorides penetrate the concrete only from the face with the specified cover depth, similar to the laboratory specimens.

Table 2
Chloride conductivity indexes (CCI) and corresponding diffusion coefficients.

Mix label	CCI (mS/cm)		Corresponding diffusion coefficient,	
	28-day	90-day	D_{28}* (cm^2/s) × 10^{-7}	D_{90}* (cm^2/s) × 10^{-10}
PC-40	1.24	1.10	25.7	47.4
FA-40	0.37	0.24	1.9×10^3	9.6
FA-55	0.89	0.70	3.2×10^3	14.8
SL-40	0.26	0.15	1.4×10^3	7.0
SL-55	0.59	0.35	1.9×10^3	8.4

* Determined based on an empirical correlation between CCI and diffusion coefficient [20].

2.5. Corrosion rate and half-cell potential measurements

Coulostatic technique was used to take corrosion rate measurements. This is a linear polarisation resistance method whereby a small charge is applied to the steel and the relaxation of potential monitored over a short period of time, to determine the polarization resistance, R_P, [26,27]. R_P is related to the corrosion current, I_{corr}, by means of the Stern-Geary coefficient B i.e. $I_{corr} = B/R_p$ where B is the Stern-Geary coefficient varying between 13 and 52 mV depending on the corrosion state of the steel (i.e. passive or active). A value of 26 mV for corroding (active) steel and of 52 mV for passive steel in the case of concrete has been established and used by a number of researchers [28–30]. In this study, therefore, a value of 26 mV was used. Corrosion current density is then expressed as: $i_{corr} = I_{corr}/A$ where A is the exposed steel surface area of approximately 86 cm^2. Data was collected using a HP 34970A data acquisition unit and analysed using a MATLAB® program.

Half-cell potential (HCP) readings, with reference to a silver/silver chloride (Ag/AgCl) reference electrode, were taken simultaneously during corrosion rate measurements. For a given exposure and test parameter, three specimens were monitored bi-weekly for corrosion rate and HCP. For each combination of binder type, cover depth and crack width, three individual specimen readings were taken and then averaged to obtain one result. In some cases, one of the three readings was eliminated (as an outlier) using Grubb's outlier test [31].

3. Results and discussion

The corrosion rate and HCP results presented in this paper are those collected during exposure of the beam specimens in their respective environments for up to 122 weeks (approximately 2¼ years). The specimen notation used in the presentation of the results is given in Fig. 5. For any corrosion rate vs. time and HCP vs. time plots presented, '*week zero*' corresponds to the time when the specimens were placed in their respective exposure environments; the first measurement was taken two weeks after exposure to the respective environments.

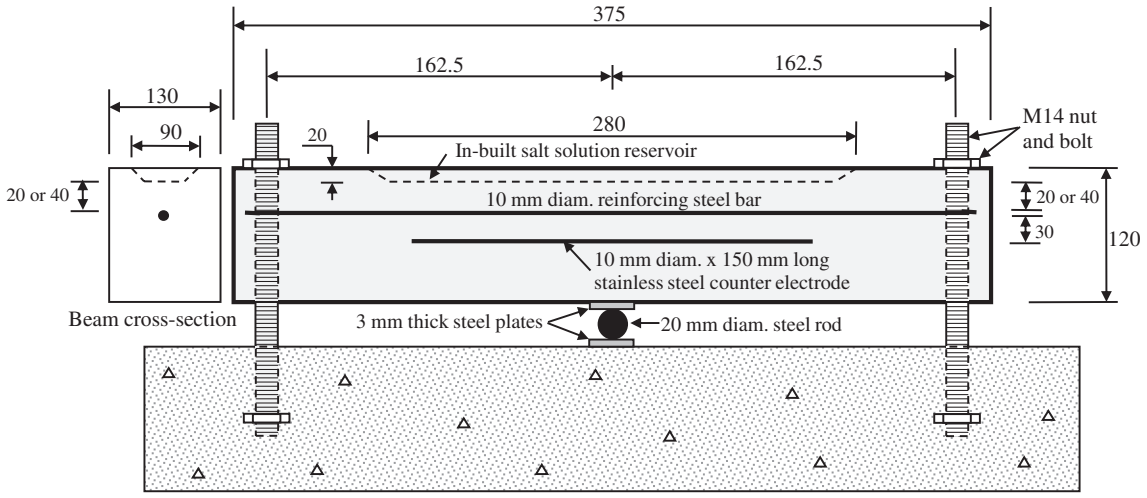

Fig. 2. Beam loading set-up for 0.4 and 0.7 mm cracked specimens.

'*Average corrosion rate*' and '*average HCP*' as used in this paper refer, respectively, to the arithmetic mean of the measured corrosion rates and HCPs between weeks 104 and 120. This time interval represented a sensible plateau phase for the time-development trends of the respective parameters. It should be noted that even though the average corrosion rates for the field specimens were also determined between weeks 104 and 120, these were not taken as the long-term stable corrosion rates as was the case for the laboratory specimens. The time development trends for corrosion rate in these specimens showed negligible increases but this was mainly attributed to the seasonal weather changes, in this case, from summer (with maximum temperatures of approximately 27 °C) to winter (with maximum temperatures of approximately 15 °C). A '2-*point moving average*' was used to represent all the corrosion rate and HCP versus time plots in order to minimize sharp kinks and make the trends distinct, but without changing the actual trends.

3.1. Early-age corrosion rate trends

Five hours after withdrawal of the IC, the measured corrosion rates in all the specimens ranged between 0.10 and 0.13 μA/cm^2; an indication that active corrosion was successfully induced. However, there were no general trends between corrosion rate and either cover depth, w/b ratio or binder type. After 2 weeks exposure in the respective environments, corrosion rates in all the specimens dropped relative to those measured after withdrawal of the IC with some specimens reverting to passive corrosion state i.e. < 0.10 μA/cm^2. No general trend was evident in the drop in corrosion rate, which varied from specimen to specimen regardless of the initial 5-hour measured corrosion rate. However, significant decreases were noted in the blended cement concrete specimens with 40 mm cover where the corrosion rates decreased to a passive state (by up to 60% in SL-40 uncracked field specimens with 40 mm cover) and in those with 20 mm cover (up to 50% in FA-40 uncracked field specimens with 20 mm cover).

The drop in corrosion rates after withdrawal of the IC and exposure to the respective environments can be attributed to one or a combination of the following phenomena:

(i) Decrease in the availability of corrosion-sustaining agents such as dissolved oxygen (especially in the uncracked specimens).
(ii) Tendency of the steel to revert to a passive corrosion state if the chloride content at the steel level is less than the chloride threshold. Even though the chloride concentration at the steel level was not measured after withdrawal of the IC due to the destructive nature of the test, it is plausible that after the 3.5 hours application of anodic IC, the chloride contents in some concretes may have not reached the threshold level.

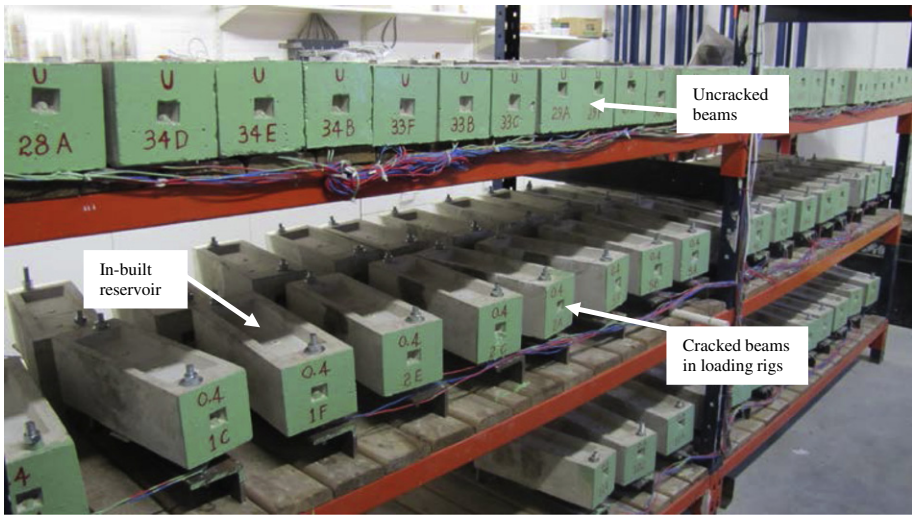

Fig. 3. Photograph showing some of the laboratory-based specimens.

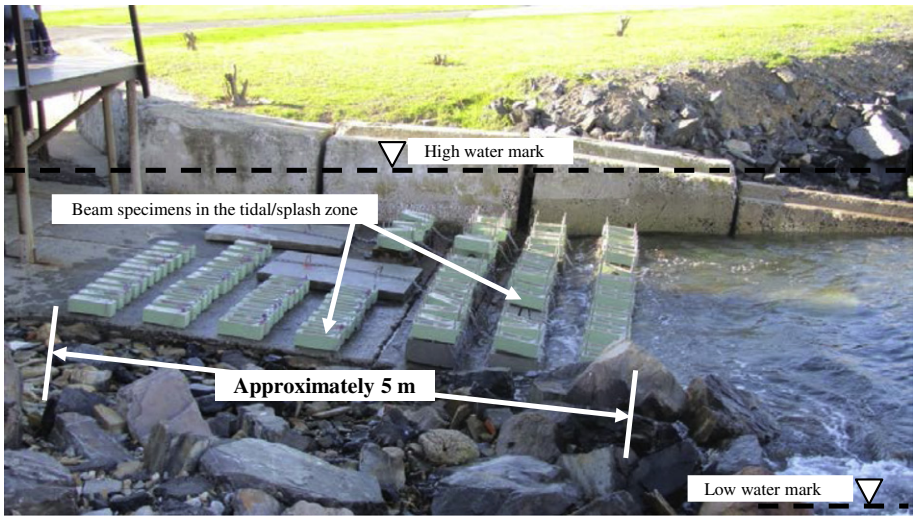

Fig. 4. Photograph showing the field-based specimens in the tidal zone.

(iii) Tendency of the corrosion rate (and potential) to decay and revert to equilibrium state (not necessarily passive corrosion state) after withdrawal of the IC.

At the end of the experimental period (122 weeks), all the specimens exhibited active corrosion.

3.2. Effect of crack width, cover depth and concrete quality on corrosion rate

3.2.1. Effect of crack width

Past studies [4–9] have shown that crack width (w_{cr}) affects corrosion rate - with increasing w_{cr} leading to increased corrosion rates but to an extent dependent on the combined effect of concrete cover, quality and resistivity. Both the laboratory and field corrosion rate results followed this trend. Typical plots are shown in Fig. 6 - note that Fig. 6(a) and (c) does not have data for incipient-cracked specimens because these were only made for 20 mm cover.

A comparison of the average corrosion rates (week 104-120) for specimens of the same exposure environment, cover depth and concrete quality (binder type and w/b ratio) but different crack widths are presented in Figs. 7 to 11. The maximum and minimum i_{corr} limits presented in these figures were obtained from a statistical analysis of the measured results ($i_{corr,max} = i_{corr,average} + 1.96\sigma$, and $i_{corr,min} = i_{corr,average} - 1.96\sigma$ where σ is the standard deviation - the value 1.96 is obtained from a standard t-distribution table at a 95% confidence interval). Furthermore, note that in Figs. 7 to 11, the following observations were inexplicable, and ascribed to experimental anomalies. They were therefore not used in the analyses:

(i) in Fig. 7(b), corrosion rate for incipient-cracked PC-40 specimen with 20 mm cover was unexpectedly higher than for 0.4 mm cracked specimens,

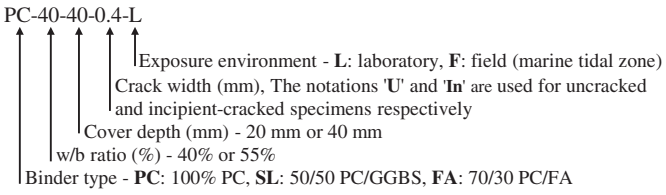

Fig. 5. Specimen notation used in the presentation of experimental results.

(ii) in Fig. 9(b), the trend between the average corrosion rate for incipient-cracked and uncracked FA-55 specimen with 20 mm cover, and

(iii) in Fig. 10(d), the statistical analysis (depicted using error bars in these figures) shows that the average corrosion rates for incipient-cracked and 0.4 mm cracked SL-40 specimens with 20 mm cover were equal.

The results show that regardless of the exposure environment, for a given binder type, w/b ratio and cover depth, corrosion rates generally increased with increase in crack width (w_{cr}) in the order uncracked → incipient-cracked → 0.4 mm cracked → 0.7 mm cracked. However, for a given exposure environment, corrosion rate at a given crack width varied depending on the combination of cover depth, binder type and w/b ratio. It must be mentioned that, for a given concrete cover and quality (binder type and w/b ratio), the increase in corrosion rate with increase in crack width is not expected to be indefinite; it is expected that there is a threshold crack width beyond which corrosion rate no longer increases. This could not be established in this study, and needs further investigation.

A summary of the effect of crack width on corrosion rate is presented in Table 3. The summary shows that in general, the presence of incipient cracks as opposed to uncracked specimens had a similar effect on corrosion rate in both the laboratory and field specimens. This was also the case for laboratory and field specimens where crack width increased from 0.4 to 0.7 mm. However, the results show that generally, increase in crack width from incipient-cracked to 0.4 mm had a relatively lesser effect on corrosion rate in the field specimens than in the corresponding laboratory ones. Even though not quantified in this study, it can be expected that, to a given degree, crack healing occurred in the incipient-cracked specimens. However, the results presented in Table 3 indicate that generally, this phenomenon may have occurred to a higher degree in the field specimens than in the laboratory ones. This can be attributed to the sealing of the cracks with debris in the sea-water. However, further studies are necessary to ascertain and quantify the assumption of crack healing and its effect on decreasing corrosion rate. The 18%, 13% and 1% (negligible) reductions in corrosion rates in, respectively, the laboratory-based PC-40 specimens with 20 mm cover, field FA-55 specimens with 20 mm cover and field SL-40 specimens with 20 mm cover due to the presence of 0.4 mm cracks are inexplicable. They were therefore not included in the general trends and conclusions drawn relating to the effect of cracking on corrosion rate. Based on this comparison (Table 3), no general trend on the effect of crack width on corrosion

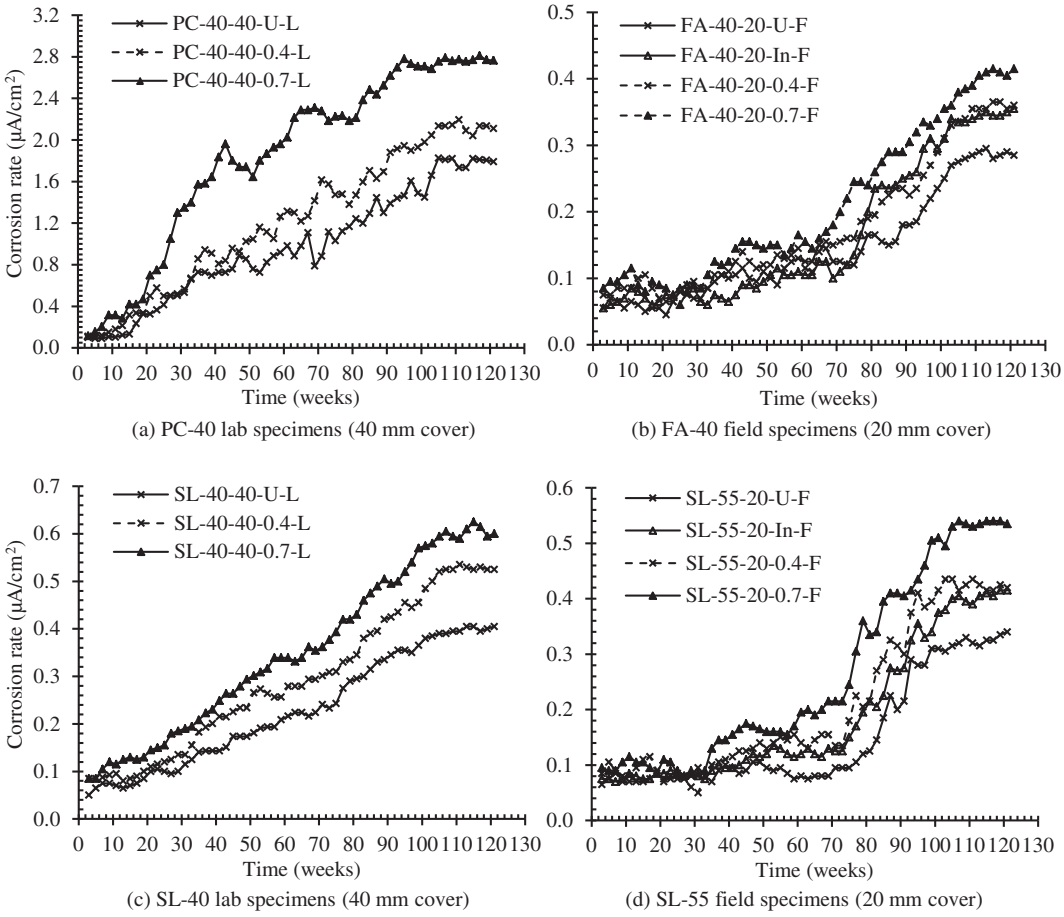

Fig. 6. Typical plots – effect of crack width on corrosion rate.

rate could be drawn between the laboratory and field specimens; in some cases, the percentage change was higher in the laboratory-based specimens while in other cases, the reverse was true.

3.2.2. Effect of cover depth

A comparison of the average corrosion rates for laboratory and field specimens with 20 and 40 mm cover depths is presented in Figs. 12 to 14. These figures also depict the influence of binder type and w/b ratio on corrosion rate which will be discussed in the next section. The results show that for a given combination of binder type, w/b ratio and crack width, corrosion rates in both the laboratory and field specimens increased with decrease in cover depth (from 40 to 20 mm). Similar trends have been reported by Akatsuka et al. [32] and Scott and Alexander [4], and are attributed mainly to the limited oxygen availability (as cover depth increases) to sustain the cathodic reaction during corrosion by increasing its travel path from the concrete surface to the steel level. This phenomenon is applicable to both the uncracked and cracked specimens because even in the latter case, the cathodes are mainly located in the uncracked concrete regions [33]. In general, in the laboratory specimens, the highest reductions in corrosion rates as a result of increased cover depth were recorded in the blended cement concrete specimens - up to 43% in uncracked FA-55 specimens and up to 45% in 0.7 mm cracked SL-40 specimens. However, no specific trend was observed in the field specimens.

Table 4 summarizes the impact of increasing cover depth on corrosion rate. In general, in the laboratory specimens, the highest reductions in corrosion rates as a result of increased cover depth were recorded in the blended cement concrete specimens. This contradicts previous findings in a study by Scott and Alexander [4] where the highest reductions in corrosion rates as a result of increased cover depth were recorded in the plain Portland cement concretes (see Table 4). It is not clear why this trend was reversed in this study. However, this trend was not observed in the field specimens where no specific trend was evident. The 17% increase in corrosion rate due to increase in cover depth from 20 to 40 mm in the uncracked FA-55 field specimens was inexplicable. Comparing the effect of increasing cover depth in the laboratory and field specimens, Table 4 shows that in both the 0.4 and 0.7 mm cracked specimens, there was no consistent trend. However, in the uncracked specimens, the field specimens exhibited higher reductions in corrosion rate than the corresponding laboratory ones. In the previous section, we saw that in the field specimens with 20 mm cover, increase in crack width from 0 (uncracked) to incipient-cracked showed the highest percentage increase in corrosion rate compared to either an increase from incipient-cracked to 0.4 mm or 0.4 to 0.7 mm (see Table 3). These results show a dominating influence of cover depth in these specimens and that even incipient-cracks can significantly increase corrosion rate.

3.2.3. Effect of concrete quality

The term *concrete quality* is used in this paper to refer the ease of ingress of corrosion-sustaining agents (mainly oxygen and moisture). It was varied by using different binder types and w/b ratios, and quantified using the chloride diffusion coefficient obtained from the conductivity index (CCI), as discussed in the previous sections. Therefore, the diffusion coefficients of the concretes were used solely to depict the relative penetrabilities of the different concretes to corrosion-sustaining agents and not to quantify a specific transport parameter of concrete as is usually the case in Fickian-based corrosion initiation prediction models. The empirical model correlating CCI to diffusion coefficient is currently used for service life prediction based on the time to corrosion initiation [22,34] but recent studies have shown that it also exhibits a

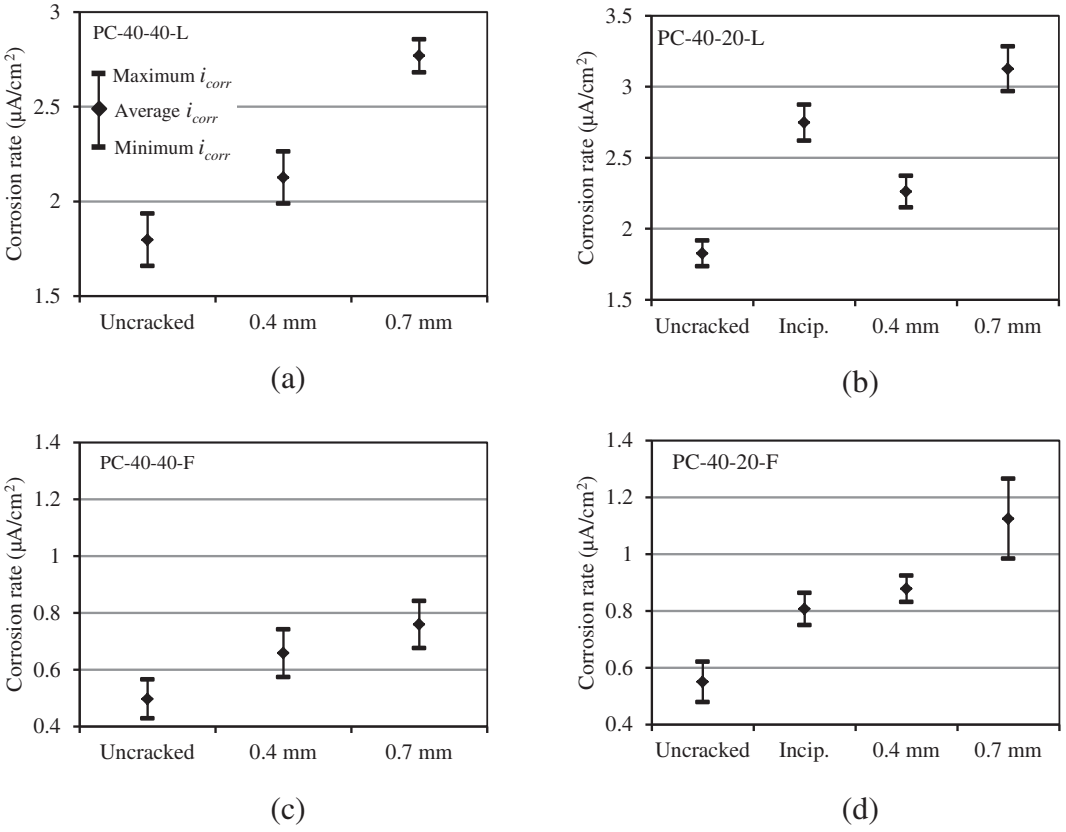

Fig. 7. Average corrosion rates in uncracked vs. cracked - PC-40 specimens.

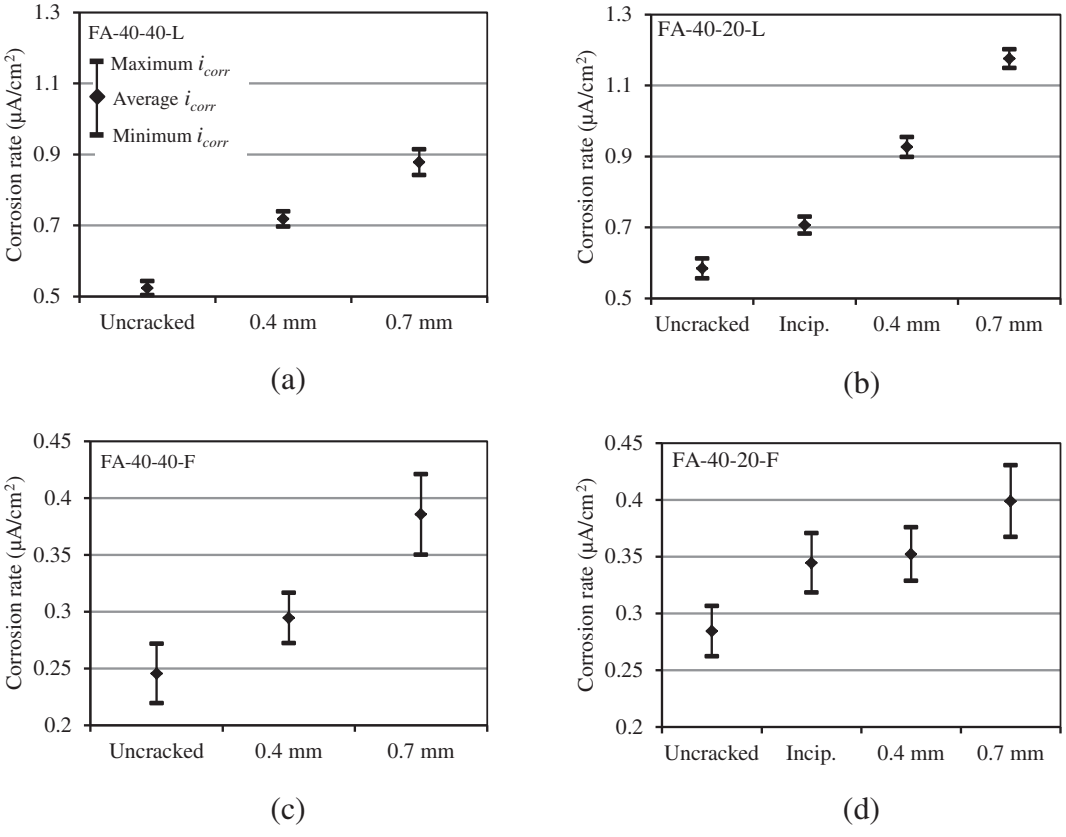

Fig. 8. Average corrosion rates in uncracked vs. cracked - FA-40 specimens.

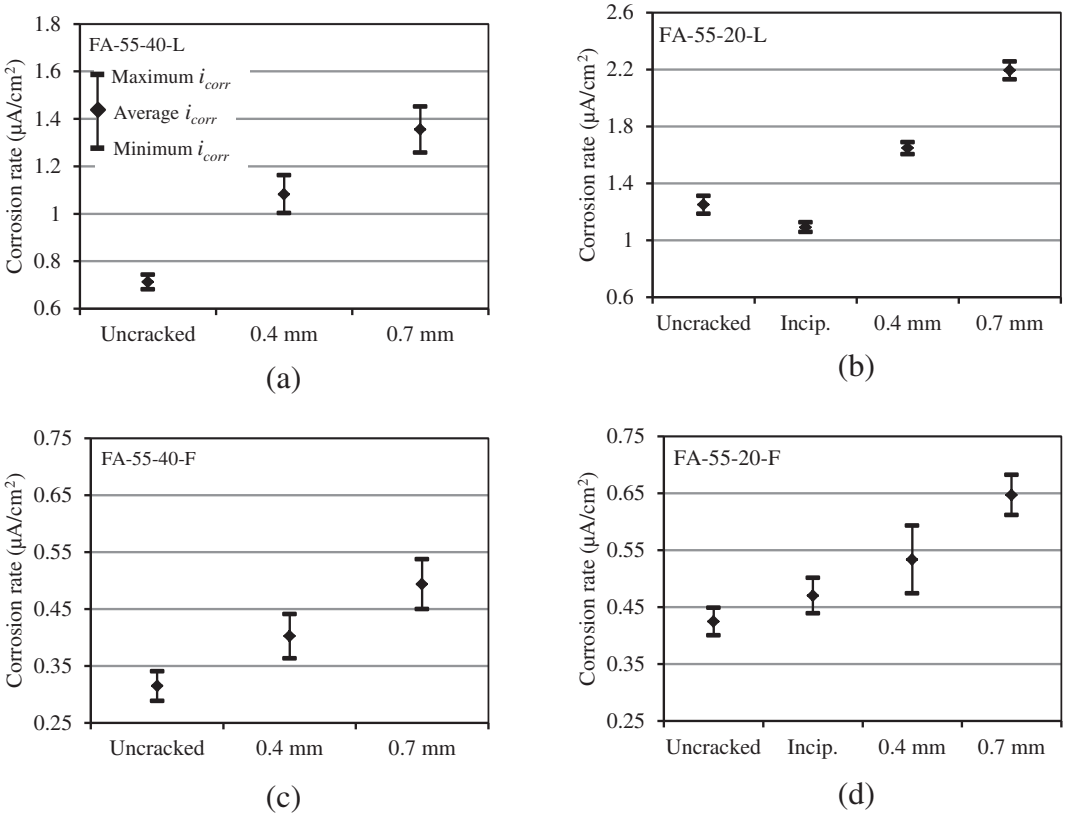

Fig. 9. Average corrosion rates in uncracked vs. cracked - FA-55 specimens.

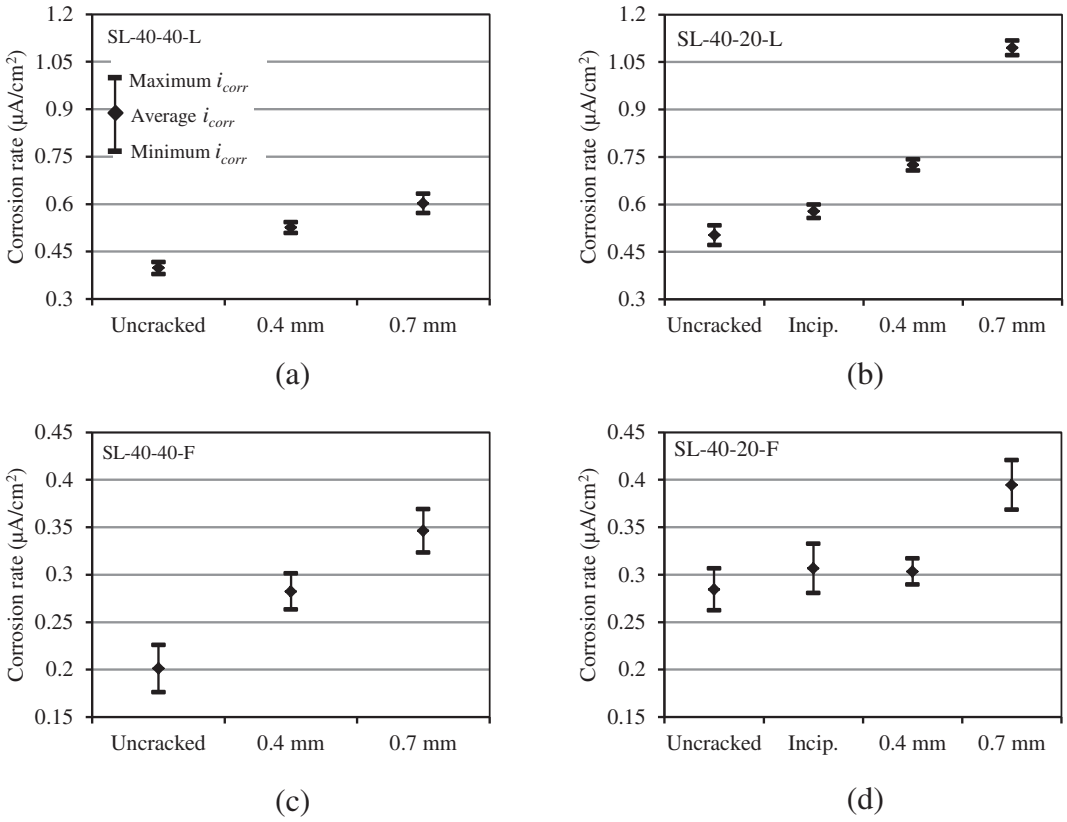

Fig. 10. Average corrosion rates in uncracked vs. cracked - SL-40 specimens.

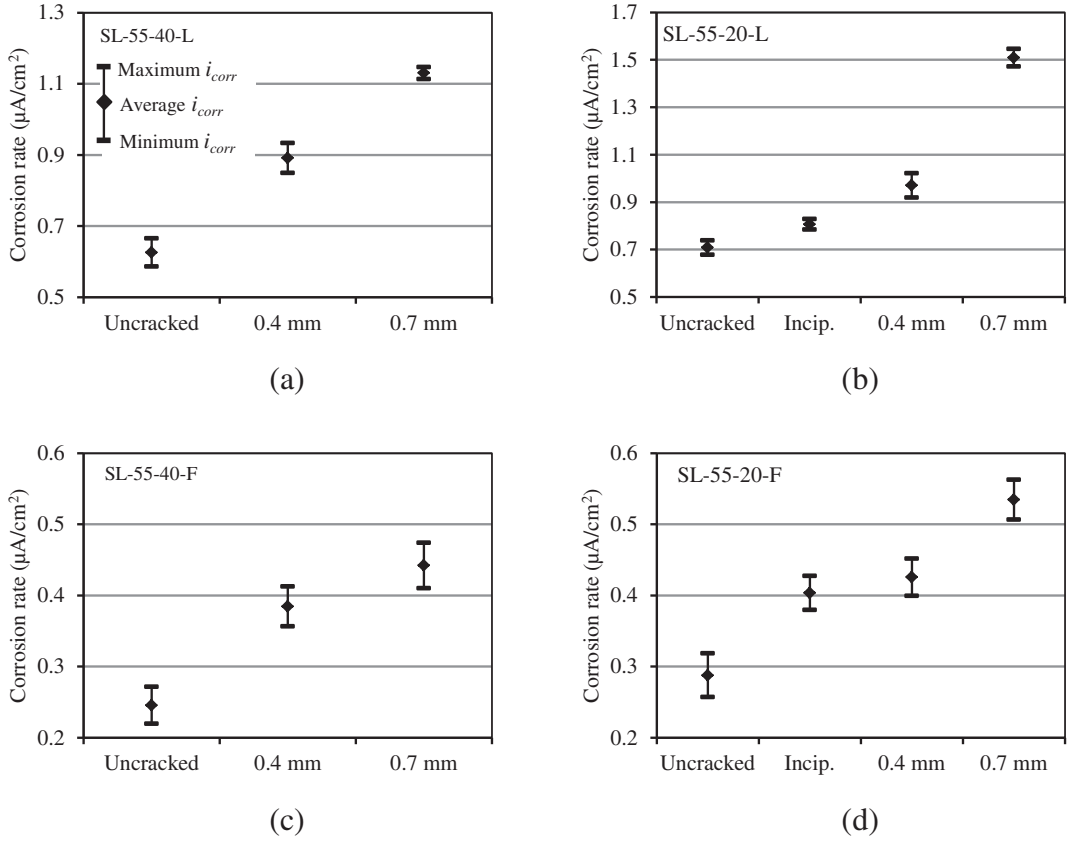

Fig. 11. Average corrosion rates in uncracked vs. cracked - SL-55 specimens.

good correlation with corrosion rate [5,35]. Concretes made using different supplementary cementitious materials, SCMs, (e.g. FA, GGBS) can exhibit the same CCI but different diffusion coefficients mainly due to differences in chloride binding capacities [20,36]. Therefore, in order to differentiate between the different binders, the equivalent diffusion coefficients of the CCI values of different binders were determined using the empirical relationship (described in previous sections) between the two parameters.

The 90-day CCI values were used to obtain the diffusion coefficients (D_{90}) used to characterize concrete quality (see Table 2), since they could account for the slower rate of maturity of the FA and GGBS blended concretes. In general, for a given binder, D_{90} values decreased with decreasing w/b ratio. As expected, the blended cement concretes had lower diffusion coefficients (hence lower penetrability) than PC concrete. This trend is attributed to the refined microstructure and higher chloride binding capacity in the blended cement concretes than in plain PC concrete [37,38].

For both cracked and uncracked specimens, the results show that concrete quality influences corrosion rate and can be used to control not only its initiation but also its propagation. Specifically, the use of blended cement concretes is more effective in controlling steel corrosion than plain PC concretes. In both laboratory and field specimens, corrosion rates for the blended cement concretes were in most cases lower those of PC concretes (Figs. 12 to 14). These results also show that for a given SCM, even though reducing the w/b ratio further decreases the concrete's quality and hence corrosion rate, the effect is small compared to that of the presence of the SCM itself. In addition, high resistivity which is a characteristic of blended cement concretes also plays a major in mitigating corrosion rate [35].

A summary of the influence of concrete quality on corrosion rate is presented in Tables 5 and 6. The effect of concrete quality on corrosion rate is compared by considering both the change in binder type for a given w/b ratio, crack width and cover depth (Table 5), and the change in w/b ratio for a given binder type, crack width and cover depth (Table 6). The latter comparison is only carried out for the fly ash and slag specimens because PC concrete was only made using 0.40 w/b ratio.

Table 5 shows that regardless of the exposure environment, for a given w/b ratio, cover depth and crack width, partial replacement of PC with either FA (30%) or GGBS (50%) led to significant reductions in corrosion rate. The results also show that there was no marked difference in the changes in corrosion rate between the field and laboratory

Table 3
Summary of the effect of cracking and crack width on corrosion rate.

Mix label	Cover (mm)	Percentage change in corrosion rate due to increase in w_{cr} (%)					
		Uncrack. → Incip. crack		Incip. crack → 0.4 mm		0.4 mm → 0.7 mm	
		Lab	Field	Lab	Field	Lab	Field
PC-40	20	+50	+47	**[b]	+9	+38	+28
	40	–*	–	–	–	+30	+15
SL-40	20	+15	+8	+25	**[c]	+51	+30
	40	–	–	–	–	+15	+23
SL-55	20	+14	+25	+20	+6	+56	+26
	40	–	–	–	–	+27	+15
FA-40	20	+21	+20	+31	+2	+27	+13
	40	–	–	–	–	+22	+31
FA-55	20	**[a]	+11	+51	+13	+33	+21
	40	–	–	–	–	+25	+23

* Note: Incipient-cracked specimens only made for 20 mm cover.
** % change in i_{corr} not included because a reduction in i_{corr} due to increase in w_{cr} was obtained.
[a]: -13%, [b]: -18%, [c]: -1%

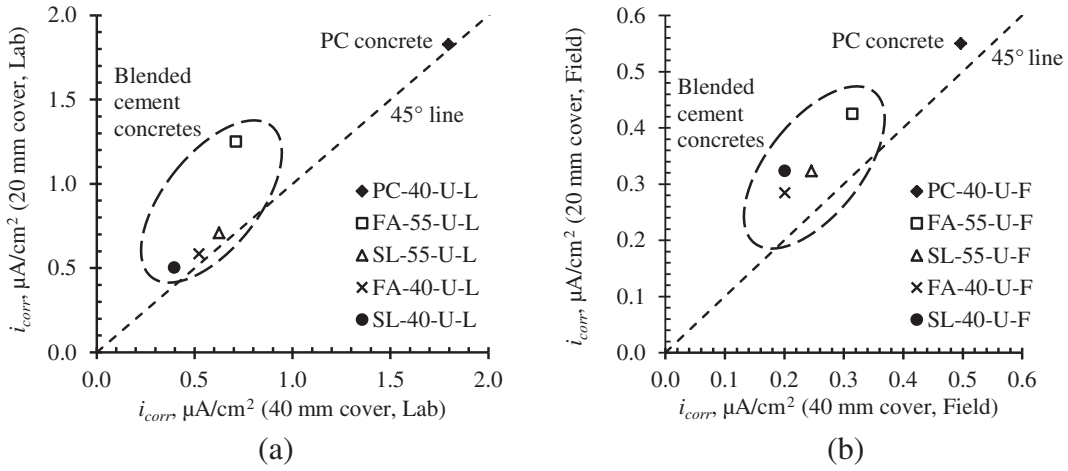

Fig. 12. Comparison of i_{corr} for 20 and 40 mm cover – uncracked specimens.

specimens due to partial replacement of PC with either FA (30%) or GGBS (50%). With respect to effect of change in concrete quality due to change in w/b ratio on corrosion rate, the analysis presented in Table 6 shows that both the blended cement concretes generally respond to changes in w/b ratio in a similar manner. Similar results have been reported in previous studies [5,39]. The effect of crack width is also evident in the analyses presented in Tables 5 and 6, especially for the 0.4 and 0.7 mm cracked specimens, but these have already been discussed in detail in previous sections.

3.3. Half-cell potential results

Typical time-development trends for HCP obtained during the experimental period are shown in Fig. 15(a) to (d). The following general trends were noted with respect to the HCP results:

(i) for a given exposure environment (laboratory or field), cover depth and crack width, the average HCP became less negative in the following order: PC-40 → FA-55 → SL-55 → FA-40 → SL-40.
(ii) HCP values for the field specimens were lower (less negative) than the laboratory ones, a trend which corresponds to that for the corrosion rate results already discussed.
(iii) for a given exposure environment, cover depth, crack width and w/b ratio, HCP values of blended cement concrete specimens were less negative than those of plain PC concrete specimens.

In general, HCP results for both the field and laboratory specimens showed a good correlation with corrosion rate i.e. higher corrosion rates corresponded to more negative HCP values (Fig. 16).

4. General discussion

The results obtained in this study have corroborated those in previous studies – cover depth, concrete quality and crack width all affect corrosion rate. In the presence of cover cracking, corrosion rate is increased but to an extent dependent on concrete cover and quality. However, it is also logical to acknowledge that even though corrosion rate increases with an increase in crack width, this trend cannot be indefinite. Other factors being constant, there will be a maximum crack width beyond which corrosion rate is no longer dependent on the increase in crack width. This could not be established in this study due to the limited number of crack widths used, and further studies are required to ascertain this hypothesis.

Concrete quality can be improved by, in addition to good construction practices (e.g. adequate compaction and proper curing), reduction

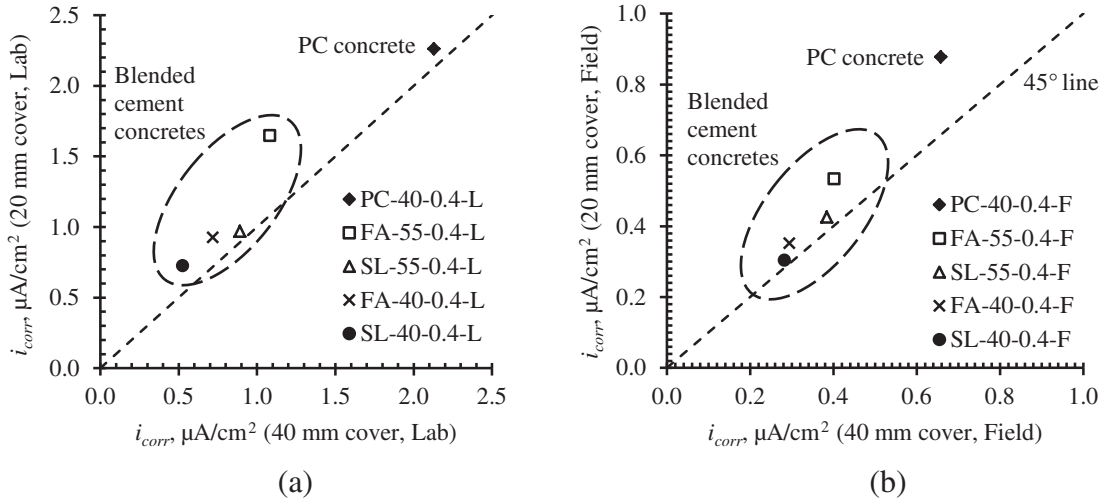

Fig. 13. Comparison of i_{corr} for 20 and 40 mm cover – 0.4 mm cracked specimens.

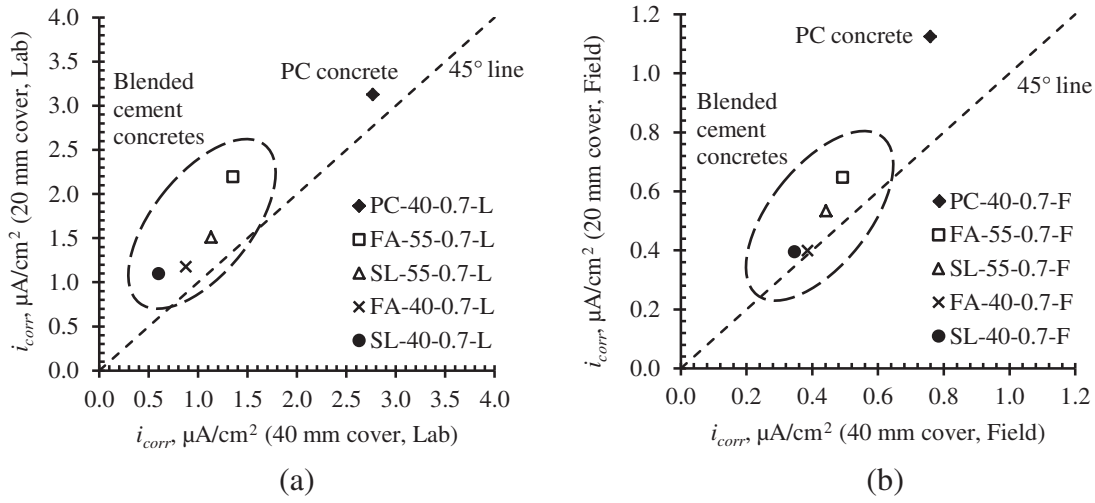

Fig. 14. Comparison of i_{corr} for 20 and 40 mm cover – 0.7 mm cracked specimens.

in w/b ratio or the replacement of plain Portland cement (PC) with SCMs such as FA and GGBS. The results from both the field and laboratory corrosion investigations indicate that the partial replacement of PC with SCMs resulted in significant reductions in corrosion rate - up to 78% and 65% in, respectively, slag (laboratory 0.7 mm cracked, 40 mm cover), and slag and fly ash (field 0.4 and 0.7 mm cracked, 20 mm cover). However, for a given w/b ratio, the blended cement concrete specimens had similar corrosion rates i.e. the corrosion performance of the blended cement concretes were less affected than PC concrete by the reduction in w/b ratio from 0.55 to 0.40. Even though only one w/b ratio (0.40) was used for the PC concrete, a previous study by Otieno et al. [5] showed similar results for blended cement concretes and higher changes in quality of PC concretes due to change in w/b ratio from 0.55 to 0.40 than in the blended cement concretes.

The results have also highlighted the need to carry out, in addition to accelerated corrosion tests in the laboratory, natural corrosion tests to establish the relationship between the corrosion performance of different concretes, and the extent of the effect of parameters such as cover depth and crack width on corrosion rate in the two scenarios. The results obtained in this study showed that the relationship is not straightforward. For example, no general trend on the effect of crack width on corrosion rate could be drawn between the laboratory and field specimens; in some cases, the increase was higher in the laboratory-based specimens while in other cases, the reverse was true. Furthermore, the impact of increasing cover on corrosion rate was relatively less in the field specimens than in the laboratory specimens.

Finally, it is important to comment on the pitting effect of chloride-induced corrosion especially in cracked concrete. Even though the corrosion rates reported in this paper were averaged over the whole steel surface, it must be acknowledged that this assumption leads to under-estimation of chloride-induced corrosion rates and

Table 4
Effect of increasing cover depth on corrosion rate.

Crack width	Mix label	% reduction in i_{corr} due to change in cover from 20 to 40 mm (at constant w_{cr})	
		Lab specimens	Field specimens
Uncracked	PC-40	2	10
	SL-40	21	33
	SL-55	12	24
	FA-40	10	30
	FA-55	43	-17
0.4 mm	PC-40	6	25
	SL-40	27	7
	SL-55	8	10
	FA-40	23	16
	FA-55	34	25
0.7 mm	PC-40	11	33
	SL-40	45	12
	SL-55	25	17
	FA-40	25	3
	FA-55	38	24

Table 5
Effect of change in binder type on corrosion rate.

Crack width and exposure		Percentage reduction in i_{corr} due to change in binder type (at a constant w/b ratio and cover)			
		PC-40 → FA-40		PC-40 → SL-40	
		20 mm	40 mm	20 mm	40 mm
Uncracked	Lab	68	71	73	78
	Field	48	60	48	62
Incipient crack	Lab	74	–*	79	–
	Field	57	–	62	–
0.4 mm	Lab	59	66	68	75
	Field	60	55	65	57
0.7 mm	Lab	62	68	65	78
	Field	65	49	65	54

* Incipient-cracked specimens were only made with 20 mm cover.

Table 6
Effect of change in w/b ratio on corrosion rate.

Crack width and exposure		Percentage reduction in i_{corr} due to change in w/b ratio (for a given binder type and cover)			
		FA-55 → FA-40		SL-55 → SL-40	
		20 mm	40 mm	20 mm	40 mm
Uncracked	Lab	53	27	29	36
n	Field	32	60	12	23
Incipient crack	Lab	35	–*	28	–
	Field	27	–	24	–
0.4 mm	Lab	44	27	25	41
	Field	34	35	29	27
0.7 mm	Lab	46	22	27	47
	Field	38	22	26	22

* Incipient-cracked specimens were only made with 20 mm cover.

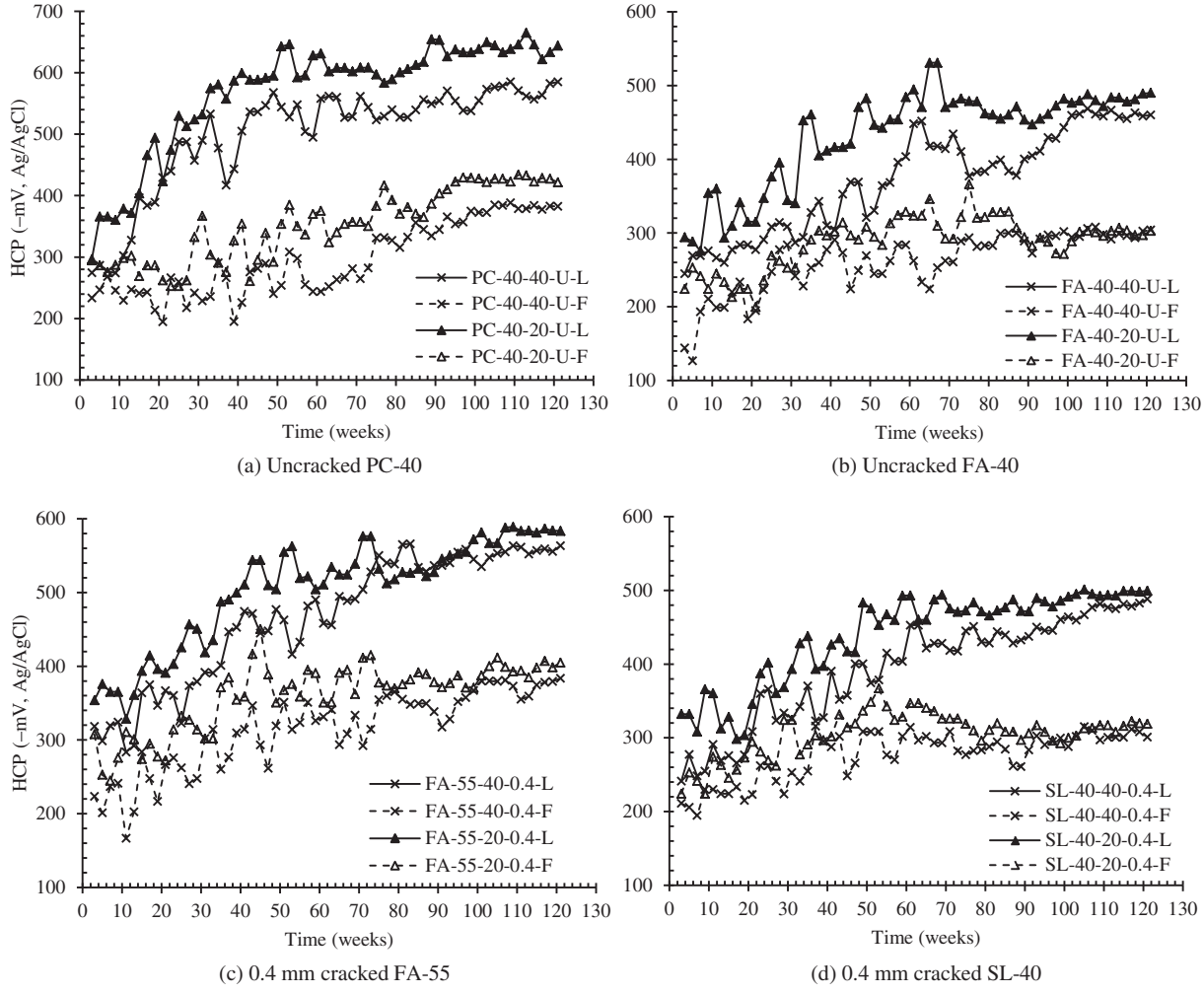

Fig. 15. Typical half-cell potential time-development trends.

consequently, the penetration depths obtained using such corrosion rates are also under-estimated. This is important especially for cracked RC where high local pitting occurs in the crack region. To account for this, pitting factors are usually introduced. Gravimetric mass loss measurements will be carried out at a later stage and compared with those calculated using the corrosion rate results reported here to quantify, if any, the error in the coulostatic linear polarization resistance measurements.

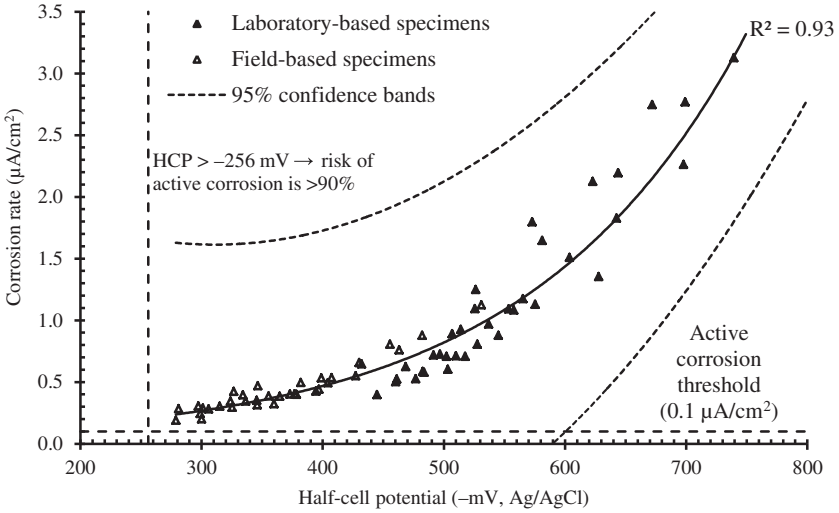

Fig. 16. Relationship between average corrosion rate and half-cell potential (all specimens).

5. Conclusions

The following conclusions can be made from the experimental results presented in this paper:

1. For a given concrete quality (binder type and w/b ratio), cover depth and exposure environment, corrosion rate increased with increasing crack width.
2. For a given binder type, crack width and cover depth, corrosion rate increased with increase in w/b ratio. However, for a given cover depth, the corrosion rates in the blended cement concrete specimens were less affected than in PC concrete specimens by the change in w/b ratio from 0.55 to 0.40. The effect of change in w/b ratio generally had a similar effect (i.e. decrease) on corrosion rate in both the field and laboratory specimens.
3. For a given w/b ratio, cover depth and crack width, partial replacement of PC with a supplementary cementitious material, SCM, (30% FA or 50% GGBS) resulted in decrease in corrosion rate. There was no marked difference in the decreases in corrosion rate between the field and laboratory specimens due to partial replacement of plain PC with SCM.
4. For a given crack width and concrete quality, corrosion rate increased with decreasing cover depth. However, in the presence of cover cracking, the impact of increasing cover depth can be substantially reduced, as was the case especially in the field specimens with 0.4 and 0.7 mm crack widths where, for a given concrete, corrosion rates in the specimens were similar for both 20 and 40 mm cover depths.
5. The corrosion performance of concretes in the field under natural corrosion cannot be inferred from its performance in the laboratory under accelerated corrosion. Other factors such as corrosion process, which were not considered in this study, should be taken into account.

Acknowledgements

The authors wish to acknowledge with gratitude the financial support over the period of this work (2009-2013) received from: The University of Cape Town, the erstwhile Cement and Concrete Institute (C&CI), The National Research Foundation (NRF), Sika (SA) Pty Ltd., PPC Ltd, AfriSam, The Tertiary Education Support Programme (TESP) of ESKOM, and the Water Research Commission (WRC).

References

[1] P. Locoge, M. Massat, J.P. Olliver, C. Richet, Ion diffusion in micro-cracked concrete, Cem. Concr. Res. 22 (2-3) (1992) 431–438.
[2] H.R. Samaha, K.C. Hover, Influence of microcracking on the mass transport properties of concrete, ACI Materials Journal 89 (4) (1992) 416–424.
[3] A. Bentur, S. Diamond, N. Berke, Steel corrosion in concrete, Fundamentals and Civil Engineering Practice. , E & FN Spon, London, 1997 41–43.
[4] A.N. Scott, M.G. Alexander, The influence of binder type, cracking and cover on corrosion rates of steel in chloride-contaminated concrete, Mag. Concr. Res. 59 (7) (2007) 495–505.
[5] M.B. Otieno, M.G. Alexander, H.-D. Beushausen, Corrosion in cracked and uncracked concrete - influence of crack width, concrete quality and crack re-opening, Mag. Concr. Res. 62 (6) (2010) 393–404.
[6] K. Pettersson, O. Jorgensen, The effect of cracks on reinforcement corrosion in high-performance concrete in a marine environment, Third ACI/CANMET Int. conference on the Performance of Concrete in Marine Environment. St. Andrews, Canada 1996, pp. 185–200.
[7] K. Suzuki, Y. Ohno, S. Praparntanatorn, H. Tamura, Mechanism of steel corrosion in cracked concrete, in: C. Page, K. Treadaway, P. Bramforth (Eds.), Corrosion of reinforcement in concrete, Society of Chemical Industry, London 1990, pp. 19–28.
[8] M. Raupach, Chloride-induced macrocell corrosion of steel in concrete - theoretical background and practical consequences, Constr. Build. Mater. 10 (5) (1996) 329–338.
[9] T. Miyagawa, Early chloride corrosion of reinforcing steel in concrete(PhD Thesis) Department of civil engineering, University of Kyoto, 1985.
[10] T.A. El Maaddawy, K.A. Soudki, Effectiveness of impressed current technique to simulate corrosion of steel reinforcement in concrete, ASCE J. Mater. Civ. Eng. 15 (1) (2003) 41–47.
[11] Y. Ballim, J.C. Reid, Reinforcement corrosion and the deflection of RC beams - an experimental critique of current test methods, Cem. Concr. Compos. 25 (6) (2003) 625–632.
[12] P.S. Mangat, M.S. Elgarf, Flexural strength of concrete beams with corroding reinforcement, ACI Struct. J. 96 (1) (1999) 149–158.
[13] J. Cairns, Y. Dut, D. Law, Structural performance of corrosion-damaged concrete beams, Mag. Concr. Res. 60 (5) (2008) 359–370.
[14] J.G. Cabrera, Deterioration of concrete due to reinforcement steel corrosion, Cem. Concr. Compos. 18 (1) (1996) 47–59.
[15] S. Jaggi, H. Bohni, B. Elsener, Macrocell corrosion of steel in concrete - experiments and numerical modelling, Eurocorr 2001. 1st - 4th Octpber, Milan, Italy2001 (11 pp.).
[16] S. Joiret, M. Keddam, X.R. Novoa, M.C. Perez, C. Tangel, H. Takenouti, Use of EIS, ring-disk electrode, EQCM and Raman spectroscopy to study the film of oxides formed on iron in 1 M NaOH, Cem. Concr. Compos. 24 (1) (2002) 7–15.
[17] C.A. Clear, Cement and Concrete Association, Technical Report No. 5591985 (England).
[18] A.M. Neville, Autogenous healing - a concrete miracle? Concr. Int. 24 (11) (2002) 76–82.
[19] N. Hearn, A recording permeameter for measuring time-sensitive permeability of concrete, in: S. Mindess (Ed.) Advances in Cementitious Materials (Ceramic Transactions), vol. 16, Published by the American Ceramic Society 1991 July, pp. 463–475 (ISBN-13: 978-0944904336).
[20] J.R. Mackechnie, Predictions of reinforced concrete durability in the marine environment, Research Monograph No. 1. , Department of civil engineering, University of Cape Town and the University of Witwatersrand, 2001.
[21] J.R. Mackechnie, Predictions of reinforced concrete durability in the marine environment(PhD Thesis) Department of civil engineering, University of Cape Town, 1996.
[22] M.G. Alexander, Y. Ballim, K. Stanish, A framework for use of durability indexes in performance-based design and specifications for reinforced concrete structures, Mater. Struct. 41 (5) (2008) 921–936.
[23] P.E. Streicher, M.G. Alexander, A chloride conduction test for concrete, Cem. Concr. Res. 25 (6) (1995) 1284–1294.
[24] C. Alonso, M. Castellote, C. Andrade, Chloride threshold dependence of pitting potential of reinforcements, Electrochim. Acta 47 (21) (2002) 3469–3481.
[25] E.E. Stansbury, R.A. Buchanan, Fundamentals of Electrochemical Corrosion, ASM International, Ohio, 2000.
[26] G. Glass, C. Page, N. Short, S. Yu, An investigation of galvanostatic transient methods used to monitor the corrosion rate of steel in concrete, Corros. Sci. 35 (5-8) (1993) 1585–1592.
[27] A. Hassanien, G. Glass, N. Buenfeld, The use of small electrochemical perturbations to assess the corrosion of steel in concrete, NDT&E Int. 31 (4) (1998) 265–272.
[28] V. Feliu, J.A. Gonzalez, S. Feliu, Corrosion estimates from transient response to a potential step, Corros. Sci. 49 (8) (2007) 3241–3255.
[29] C. Andrade, C. Alonso, Corrosion rate monitoring in the laboratory and on-site, Constr. Build. Mater. 10 (5) (1996) 315–328.
[30] J.A. Gonzalez, J.M. Miranda, S. Feliu, Consideration on the reproducibility of potential and corrosion rate measurements in reinforced concrete, Corros. Sci. 46 (10) (2004) 2467–2485.
[31] F.E. Grubbs, Procedures for detecting outlying observations, Army Statistics Manual DARCOM-P706-103. , U.S. Army Research and Development Center, Aberdeen Proving Ground, MD, 1979 (21005).
[32] Y. Akatsuka, H. Seki, K. Asaoka, Crack width and reinforcement corrosion in reinforced concrete attacked by sea-water, Cem. Concr. Assoc. 266 (January) (1966) 38–43.
[33] P. Schießl, M. Raupach, Laboratory studies and calculations on the influence of crack width on chloride-induced corrosion of steel in concrete, ACI Mater. J. 94 (1) (1997) 56–62.
[34] R. Muigai, P. Moyo, M. Alexander, Durability design of reinforced concrete structures: a comparison of the use of durability indexes in the deemed-to-satisfy approach and the full-probabilistic approach, Mater. Struct. 45 (8) (2012) 1233–1244.
[35] A.N. Scott, The influence of binder type and cracking on reinforcing steel corrosion in concrete(PhD Thesis) Department of civil engineering, University of Cape Town, 2004.
[36] C. Arya, N.R. Buenfeld, J.B. Newman, Factors influencing chloride binding in concrete, Cem. Concr. Res. 20 (2) (1990) 291–300.
[37] J.H. Rose, Effect of cementitious blastfurnace slag on chloride permeability of concrete, ACI Spec. Publ. 102 (September) (1987) 107–126.
[38] V.M. Malhotra, Properties of fresh and hardened concrete incorporating ground granulated blast furnace slag, in: V.M. Malhotra (Ed.), Supplementary cementing materials for concrete, Minister of Supply and Services, Canada 1987, pp. 291–336.
[39] R. Somma, C. Jaturapitakkul, W. Chalee, P. Rattanachu, Effect of the water-to-binder ratio and ground fly ash on properties of recycled aggregate concrete, J. Mater. Civ. Eng. 24 (1) (2012) 16–22.